Structure of the acetone liquid/vapor interface

Yuh Ling Yeh
Institute of Atomic and Molecular Sciences, Academia Sinica, P.O. Box 23-166, Taipei 10764, Taiwan

Chun Zhang and Hermann Held
Department of Physics, University of California at Berkeley, Berkeley, California 94704

A. M. Mebel
Institute of Atomic and Molecular Sciences, Academia Sinica, P.O. Box 23-166, Taipei 10764, Taiwan

Xing Wei
Department of Physics, University of California at Berkeley, Berkeley, California 94704

S. H. Lin
Institute of Atomic and Molecular Sciences, Academia Sinica, P.O. Box 23-166, Taipei 10764, Taiwan

Y. R. Shen[a)]
Department of Physics, University of California at Berkeley, Berkeley, California 94704

(Received 9 August 2000; accepted 27 October 2000)

The structure of the liquid/vapor interface of acetone is investigated theoretically by molecular dynamics simulation and experimentally by infrared-visible sum frequency vibrational spectroscopy. The simulation yields the molecular orientational distribution at the liquid surface. In conjunction with the *ab initio* calculation, the sum-frequency vibrational spectra for the interface is then computed, allowing a direct comparison to the measured spectra. As the calculation agrees well with the experiment, we can conclude that the molecules at the liquid surface are polar ordered, with one of the methyl groups pointing away from the bulk and the molecular plane perpendicular to the surface. This orientation is similar to that of molecules in the layer planes of crystalline acetone. Together with the appreciable surface tension of acetone, it suggests that the acetone liquid surface has a more ordered structure than the bulk and is more or less crystal-like. © *2001 American Institute of Physics.* [DOI: 10.1063/1.1333761]

I. INTRODUCTION

The study of interfacial properties of liquids is important because of its direct relevance to the chemical reactivity of the system; for example,[1] the isomerization reaction at aqueous interfaces, ion solvation at liquid interfaces, interfacial charge transfer and electron transfer reactions, atmospheric and environmental chemistry, wetting, weathering, and biological phenomena. The asymmetric environment of a liquid surface is significantly different from the isotropic environment of a liquid bulk. Numerous experimental and computational studies of the processes mentioned above indicate that surface structure and properties of the liquid and their effects on the processes must be considered at the microscopic level.

In recent years, progress in both experimental and computational approaches of studies of liquid interfaces has significantly enhanced our understanding of chemical reactivity at liquid interfaces from the microscopic point of view. On the experimental side, in addition to the many methods that have been used for the study of bulk systems and datable to the study of interfaces, a number of surface-specific techniques have been developed. Among these, infrared-visible sum frequency vibrational spectroscopy (SFVS)[2–4] has been proven to be a powerful tool to probe the orientation distribution of the interfacial molecules. On the theoretical side, molecular dynamics (MD) simulation has provided insight to the structure and the dynamical processes for liquid interfacial systems.[5,6] With the optical parameters of a single molecule obtained from an *ab initio* calculation and the molecular orientational distribution at the interface obtained from MD simulation, one can also compute SFVS spectra, and directly compare with the experimental spectra.[7]

In this work, we are interested in the liquid/vapor interface of acetone. Acetone is one of the most important aprotic dipolar organic solvents. Each molecule contains two methyl groups, symmetrically connected to a C═O double bond. The bulk structure of acetone has been examined by both experiments and simulations,[8] but the surface structure has not yet been investigated. Here, we report the results of our *ab initio* calculation, MD simulation, and SFVS measurement on the vapor/acetone interface. We will show that the molecules at the interface are polar ordered, with one of the methyl groups pointing away from the bulk and the molecular plane more or less perpendicular to the surface. This orientation is similar to that of acetone molecules in a crystalline layer, suggesting that the surface acetone structure is crystal-like.

II. CALCULATION

A. Molecular dynamics simulation

The coordinate systems for an acetone molecule are shown in Fig. 1(a). Its orientation in space is defined in Fig. 1(b) by three angles: θ is the tilt angle of the C═O axis (ζ

a)Electronic mail: shenyr@socrates.berkeley.edu

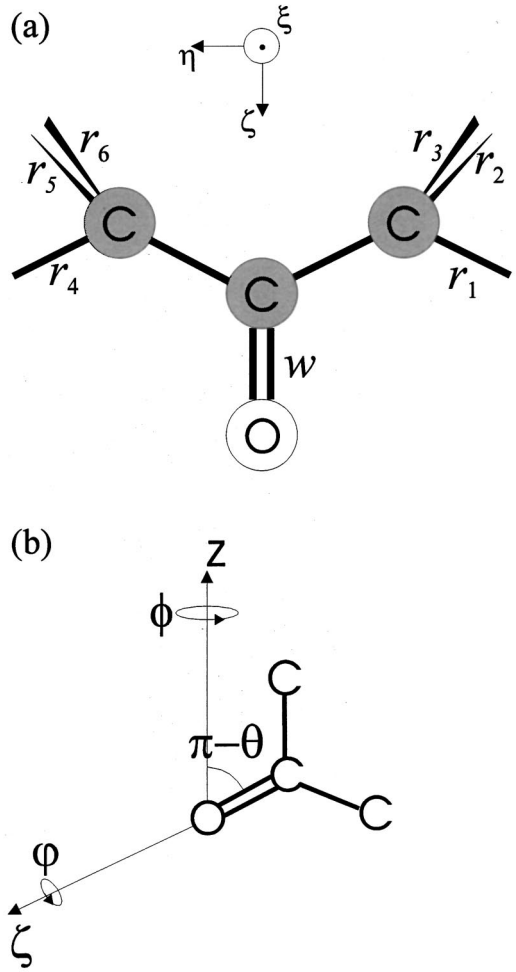

FIG. 1. Schematic diagram of an acetone molecule in (a) the molecular coordinates and (b) the lab coordinates. The stretches of six C–H bonds are defined in (a) as $r_i(i=1-6)$, respectively, and the stretch of C═O is defined in the diagram as w. The three angles (θ, φ, ϕ), used to define the molecular orientation, are labeled in (b).

axis) from the surface normal (z axis), ϕ is the azimuthal angle of the projection of the ζ axis in the x-y plane, and φ is the twist angle of the molecule (η-ζ plane) along the ζ axis. We have carried out a MD simulation (at 300 K) to obtain the orientational distribution $f(\theta,\phi,\varphi)$ for acetone molecules at the vapor/liquid interface at room temperature.

The acetone potentials employed in the simulations are the Jorgensen's optimized potential for liquid simulation (OPLS) potential[9] and the one developed by Klein and co-workers.[10] Both potentials are represented by a rigid set of four interaction sites located on oxygen and carbon atoms. The CH_3 groups are treated as unit sites. The interaction potential between two molecules is described in the standard form of Lennard-Jones (LJ) potential plus electric interaction represented by Coulomb interactions of fictitious partial charges,

$$U=\sum_{i=1}^{4}\sum_{j=1}^{4}\left\{4\epsilon_{ij}\left[\left(\frac{\sigma_{ij}}{r_{ij}}\right)^{12}-\left(\frac{\sigma_{ij}}{r_{ij}}\right)^{6}\right]+\frac{q_iq_j}{4\pi\epsilon_0 r_{ij}}\right\},$$

with

$$\epsilon_{ij}=\sqrt{\epsilon_i\epsilon_j},\quad \sigma_{ij}=\tfrac{1}{2}(\epsilon_i+\epsilon_j), \tag{1}$$

TABLE I. Intermolecular potential parameters used for acetone.

	Site	σ(Å)	ϵ/k_B (K)	q/e	Geometry
Jorgensen	C	3.910	52.87	0.300	$r_{MeC}=1.5072$ Å
	O	3.750	105.75	−0.424	$r_{CO}=1.2219$ Å
	CH_3	2.960	80.57	0.062	∠MeCMe=117.20°
Klein	C	3.75	52.84	0.566	$r_{MeC}=1.572$ Å
	O	2.96	105.68	−0.502	$r_{CO}=1.223$ Å
	CH_3	3.88	85.00	−0.032	∠MeCMe=117.3°

where r_{ij} is the distance between sites i and j in different molecules, q_i is the charge assigned to site i, and the parameters q_i, σ_i, and ϵ_i for the carbon, oxygen, and methyl sites in the acetone molecule are given in Table I. It turns out that the acetone surface structures obtained from MD simulations with Jorgensen's and Klein's potentials are virtually indistinguishable. Therefore in the following we present only results obtained with the Jorgensen's potential function.

The computer algorithm used in this work is adopted from our previous work for molecular dynamics simulations of TIP4P water.[11] The equations of motions are solved using the Leapfrog[12] algorithm with a time step of 2.0×10^{-15} s. The constraints are handled using the SHAKE[13] technique. The cutoff distance is 14 Å for OPLS potential and 20 Å for Klein's potential parameters. The system includes 512 acetone molecules in a cubic box of size 31.9 Å. The bulk box of acetone is equilibrated for a period of 200 ps in an NVT ensemble.[14] Once equilibrated, the box length in the z direction is extended to 135 Å, and this new system is equilibrated for another 200 ps in an NVT ensemble. Periodic boundary conditions are applied in all three directions. The electrostatic long-range interactions are calculated with the Ewald summation technique, as suggested by Tildesley.[15] To determine the equilibrium structure, data are calculated over a period of 400 ps and collected every five steps.

The simulation result of the density profile for acetone shown in Fig. 2 can be approximated by a hyperbolic tangent function of the form[16]

$$\rho(z)=\tfrac{1}{2}(\rho_L+\rho_V)-\tfrac{1}{2}(\rho_L-\rho_V)\tanh[(z-z_0)/d], \tag{2}$$

where ρ_L and ρ_V are the densities corresponding to the liquid and the vapor phases, $z_0=32.2$ Å is the position of the Gibb's dividing surface, and d is a parameter for the thickness of the interface. The usual definition of the surface thickness refers to the region where the density of acetone changes between 90% and 10% of the bulk value. The thickness obtained from our simulation is 5.8 Å. With long-wavelength fluctuations suppressed, the simulation result gives an accurate account of the ''intrinsic interfacial width.''[17] This means that the thickness predicted here is from the local, static spread in molecular orientation attributable to microscale molecular interactions[18] and suggests that the simulation results tends to consistently underestimate the surface thickness of a real fluid. According to the density profile shown in Fig. 2, we define three regions along z: bulk ($z<29.3$ Å), interface (29.3 Å$<z<$35.1 Å), and outer layer of the interface ($z>35.1$ Å). We then examine the orientations of the acetone molecules in these three regions.

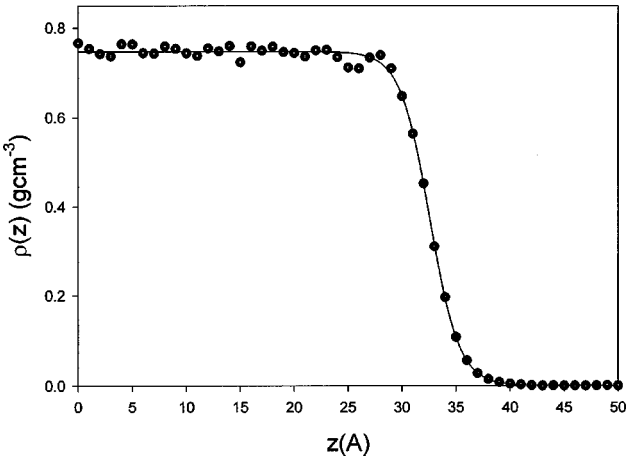

FIG. 2. Calculated density profile of 512 acetone molecules equilibrated at 300 K. Dots are from the simulation, which can be approximated by a hyperbolic tangent function (solid curve).

As shown in Fig. 3(a), in both the outer layer of the interface and the interface region, the tilt angle θ has a fairly broad distribution over 0° to 180°, i.e., 1 to -1 of cos θ. The preference of cos θ at negative values indicates that the C═O vectors of surface molecules tend to point inward into the bulk. In the bulk region, the cos θ distribution is uniform, corresponding to random orientations of the C═O vectors in the bulk. In fact, not only the C═O vector, but the whole molecule has no preference of orientation in the bulk. As a result, the twist angle φ has a uniform distribution from 0° to 360° in the bulk region [see Fig. 3(b)]. In the interface region, the most probable φ angles are 90° and 270°, corresponding to the geometry with the molecular plane (CCC plane) perpendicular to the surface. It suggests that one of the methyl groups points away from the liquid side and the other embedded in the liquid. In the outer layer of the interface, on the contrary, the most probable φ angles are 0° and 180°, indicating that the line connecting the two CH_3 sites is parallel to the surface. The simulation results for azimuthal angle ϕ is trivial. In all three regions, the angular distribution of ϕ is flat (not shown), consistent with the required azimuthal isotropy for both the bulk and the surface.

B. Molecular theory of SFVS

It has been shown[7] that the resonant part of the second-order optical nonlinear susceptibility $\chi^{(2)}$ for vibrational infrared-visible sum frequency generation (SFG) can be expressed as

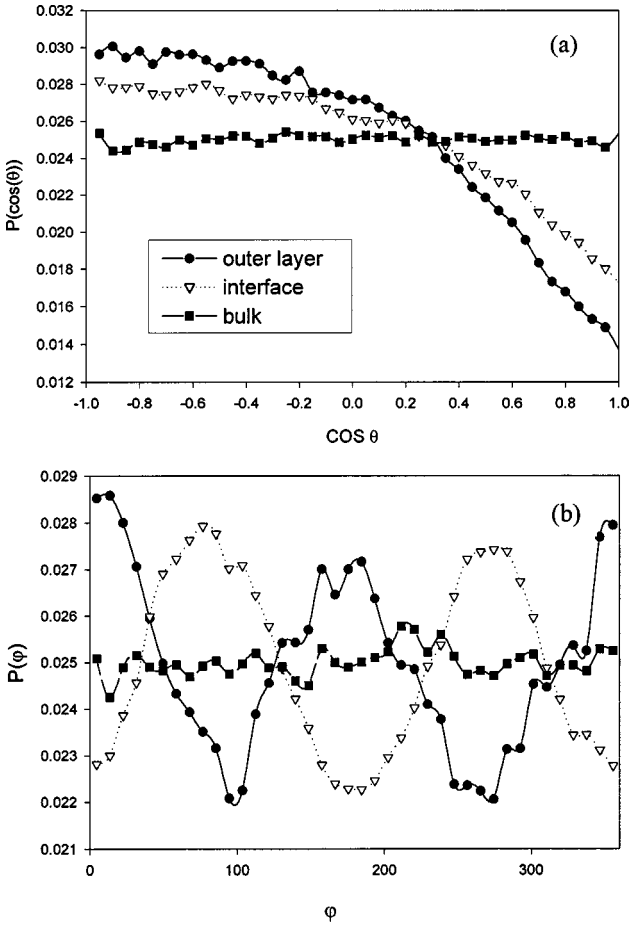

FIG. 3. Calculated orientation distributions of (a) cos θ and (b) φ of molecules in the three different regions at 300 K.

$$\chi^{(2)}_{ijk}(\omega_{IR}) = \frac{i}{\hbar^2}\sum_{\nu}\sum_{\nu'}\sum_{q}(\sigma_{\nu\nu}-\sigma_{\nu'\nu'}) \times K_{q,ijk}\frac{|\langle g\nu|Q_q|g\nu'\rangle|^2}{i(\omega_{g\nu',g\nu}-\omega_{IR})+\Gamma_{g\nu',g\nu}},$$

with

$$K_{q,ijk} \equiv \sum_{l,m,n}\langle(\mathbf{i}\cdot\mathbf{l})(\mathbf{j}\cdot\mathbf{m})(\mathbf{k}\cdot\mathbf{n})\rangle\left(\frac{\partial\alpha_{lm}}{\partial Q_q}\right)\left(\frac{\partial\mu_n}{\partial Q_q}\right). \quad (3)$$

Here, $\sigma_{\nu\nu}$ is the population in the $|g\nu\rangle$ state with g and ν denoting the ground electronic state and the associated vibrational state, respectively, Q_q is the normal coordinate of the qth vibrational mode, $\partial\alpha_{lm}/\partial Q_q$ and $\partial\mu_n/\partial Q_q$ are the infra-

TABLE II. Calculated and experimental C–H stretch vibrational frequencies and IR intensities of acetone.

Normal mode	Vibrational frequency (cm^{-1}) Theory	Experiment	IR intensity [D^2/(Å^2 amu)]
$Q_1(a_1)=12^{-1/2}(2r_1-r_2-r_3+2r_4-r_5-r_6)$	3025	3006	0.4389
$Q_2(a_1)=6^{-1/2}(r_1+r_2+r_3+r_4+r_5+r_6)$	2927	2926	0.3399
$Q_3(a_2)=4^{-1/2}(r_2-r_3-r_5+r_6)$	2973	2968	0.0
$Q_4(b_2)=12^{-1/2}(2r_1-r_2-r_3-2r_4+r_5+r_6)$	3023	3006	0.4379
$Q_5(b_2)=6^{-1/2}(r_1+r_2+r_3-r_4-r_5-r_6)$	2920	2926	0.1612
$Q_6(b_1)=4^{-1/2}(r_2-r_3+r_5-r_6)$	2980	2968	1.1815

TABLE III. Infrared dipole moment gradients, $\partial\mu_n/\partial Q_q$, of acetone in the normal coordinate basis.

Normal mode	Dipole moment gradient [D/(Å amu$^{1/2}$)]		
	μ_ξ	μ_η	μ_ζ
$Q_1(a_1)$	0	0	−0.662 530
$Q_2(a_1)$	0	0	−0.583 019
$Q_3(a_2)$	0	0	0
$Q_4(b_2)$	0	−0.661 735	0
$Q_5(b_2)$	0	0.401 469	0
$Q_6(b_1)$	−1.086 960	0	0

red dipole moment gradient and Raman polarizability for the qth vibrational mode, $\omega_{g\nu',g\nu}$ and $\Gamma_{g\nu',g\nu}$ are the resonance frequency and damping constant, and **i**, **j**, **k** refer to the lab coordinates and **l**, **m**, **n** to the molecular coordinates. The angular brackets in the expression of $K_{q,ijk}$ denote an orientational average with the prescribed orientational distribution.[19,20]

In this study, we consider only CH stretch vibrational modes Q_q (with $q=1-6$) of individual acetone molecules[21] (see Table II). For these modes, $\partial\alpha_{lm}/\partial Q_q$ and $\partial\mu_n/\partial Q_q$ in Eq. (3) are computed with an *ab initio* calculation. At the CASSCF and HF 6-311G** levels,[22] we obtain the numerical values shown in Tables III and IV.

Being a rank-3 tensor, $\chi^{(2)}$ has, in general, 27 elements. However, one can use the symmetry of the interface to reduce the number of independent elements. As a liquid surface is azimuthally isotropic (uniaxial), there are only four independent nonvanishing elements in $\chi^{(2)}$. In addition, if the visible input beam is not on resonance, $\chi_{ijk}\cong\chi_{jik}$ because the Raman polarizability tensor is approximately symmetric. Then there are only three nonvanishing independent $\chi^{(2)}$ elements. With the lab coordinates chosen such that z is along the interface normal and x in the incidence plane, they are $\chi_{yyz}=\chi_{xxz}$, $\chi_{yzy}=\chi_{zyy}=\chi_{xzx}=\chi_{zxx}$, and χ_{zzz}.[19]

To compare the calculation with the experiment, we note that the SF signal with a selected set of input/output polarization combination (**i**, **j**, **k**) is given by

$$S\propto|(\chi^{(2)}_{\mathrm{eff}})_{ijk}|^2=|L_{ii}(\omega_{\mathrm{SF}})\chi^{(2)}_{ijk}L_{jj}(\omega_{\mathrm{VIS}})L_{kk}(\omega_{\mathrm{IR}})|^2, \quad (4)$$

where $L_{ii}(\Omega)$ is the overall local-field correction factor at Ω (listed in Appendix B).[20] Calculation of $|\chi^{(2)}_{\mathrm{eff},ijk}(\omega_{\mathrm{SF}}=\omega_{\mathrm{VIS}}+\omega_{\mathrm{IR}})|^2$ allows a direct comparison with the measured SFVS spectrum.

With the input and output beams being either s or p polarized, there are eight different input/output polarization combinations. Because a liquid surface is azimuthally isotropic, SFG in SSS, SPP, PSP, PPS combinations vanish. The effective nonlinear susceptibilities under the other four polarization combinations can be expressed as[20]

$$\begin{aligned}
\chi^{(2)}_{\mathrm{eff,SSP}}&=\sin\beta_{\mathrm{IR}}L_{yy}(\omega_{\mathrm{SF}})L_{yy}(\omega_{\mathrm{VIS}})L_{zz}(\omega_{\mathrm{IR}})\chi_{yyz},\\
\chi^{(2)}_{\mathrm{eff,SPS}}&=\sin\beta_{\mathrm{VIS}}L_{yy}(\omega_{\mathrm{SF}})L_{zz}(\omega_{\mathrm{VIS}})L_{yy}(\omega_{\mathrm{IR}})\chi_{yzy},\\
\chi^{(2)}_{\mathrm{eff,PSS}}&=\sin\beta_{\mathrm{SF}}L_{zz}(\omega_{\mathrm{SF}})L_{yy}(\omega_{\mathrm{VIS}})L_{yy}(\omega_{\mathrm{IR}})\chi_{yzy},
\end{aligned} \quad (5)$$

$$\begin{aligned}
\chi^{(2)}_{\mathrm{eff,PPP}}=&-\cos\beta_{\mathrm{SF}}\cos\beta_{\mathrm{VIS}}\sin\beta_{\mathrm{IR}}L_{xx}(\omega_{\mathrm{SF}})L_{xx}(\omega_{\mathrm{VIS}})\\
&\times L_{zz}(\omega_{\mathrm{IR}})\chi_{yyz}+\sin\beta_{\mathrm{SF}}\sin\beta_{\mathrm{VIS}}\sin\beta_{\mathrm{IR}}\\
&\times L_{zz}(\omega_{\mathrm{SF}})L_{zz}(\omega_{\mathrm{VIS}})L_{zz}(\omega_{\mathrm{IR}})\chi_{zzz}\\
&-\cos\beta_{\mathrm{SF}}\sin\beta_{\mathrm{VIS}}\cos\beta_{\mathrm{IR}}L_{xx}(\omega_{\mathrm{SF}})L_{zz}(\omega_{\mathrm{VIS}})\\
&\times L_{xx}(\omega_{\mathrm{IR}})\chi_{yzy}+\sin\beta_{\mathrm{SF}}\cos\beta_{\mathrm{VIS}}\\
&\times\cos\beta_{\mathrm{IR}}L_{zz}(\omega_{\mathrm{SF}})L_{xx}(\omega_{\mathrm{VIS}})L_{xx}(\omega_{\mathrm{IR}})\chi_{yzy},
\end{aligned}$$

where β_{SF}, β_{VIS}, and β_{IR} are the reflection or incidence angles of the SF, visible, and infrared beams, respectively.

With the molecular orientational distribution obtained from MD simulation, we can now calculate the SFVS spectra ($\propto|\chi^{(2)}_{\mathrm{eff}}|^2$) of the vapor/liquid interface of acetone using Eqs. (3)–(5). We average the contributions from all molecules in the simulation box and find the SSP, SPS, PSS, and PPP spectra. As shown in Fig. 4, the calculation gives a strong peak in the SSP spectrum at 2926 cm^{-1} and a weak peak at 2968 cm^{-1}. For PPP, the peak at 2926 cm^{-1} appears to be two times weaker than that in SSP. For other polarization combinations, the peaks are all relatively weak.

Being a second-order process, SFG is highly surface specific and has a submonolayer sensitivity. The SFVS spectra obtained above mainly arise from molecules in the interface region. This is seen in Fig. 5, where the calculated SF output per molecule from each 1 Å slab parallel to the interface in the simulation box is presented as a function of the slab position. Indeed the dominant contribution comes from molecules in the interface region.

TABLE IV. Raman polarizability, $\partial\alpha_{lm}/\partial Q_q$, of acetone in the normal coordinate basis, calculated at $\lambda=300$ nm.

Normal mode	Polarizability gradient (Å^2/amu$^{1/2}$)						Raman intensity (Å^4/amu)
	$\alpha_{\xi\xi}$	$\alpha_{\eta\eta}$	$\alpha_{\zeta\zeta}$	$\alpha_{\xi\eta}$	$\alpha_{\eta\zeta}$	$\alpha_{\xi\zeta}$	
$Q_1(a_1)$	2.116 789	−2.136 330	1.059 473	0	0	0	0.120 162
$Q_2(a_1)$	2.523 211	2.581 069	2.948 260	0	0	0	7.204 821
$Q_3(a_2)$	0	0	0	0.687 684	0	0	0
$Q_4(b_2)$	0	0	0	0	1.841 603	0	0
$Q_5(b_2)$	0	0	0	0	0.490 021	0	0
$Q_6(b_1)$	0	0	0	0	0	−2.900 096	0

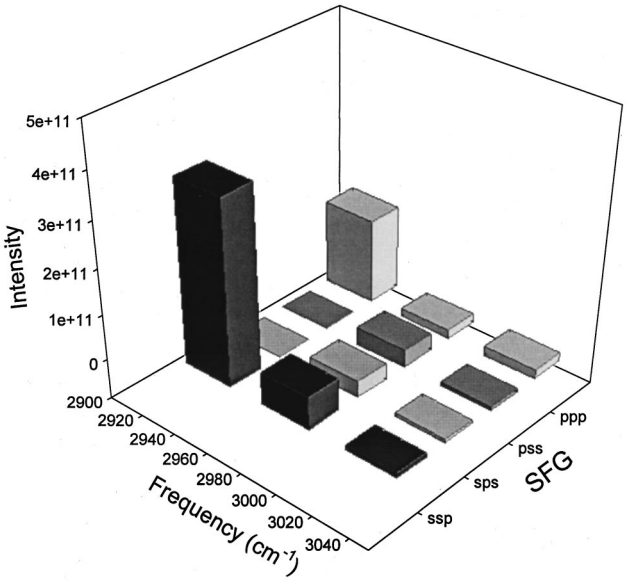

FIG. 4. Calculated SF vibrational spectra for C–H stretches of acetone molecules in the simulation box at 300 K.

III. EXPERIMENT

The SFG experimental setup has been described elsewhere.[23] In this experiment, a visible beam at 532 nm and an IR beam tunable from 1.2 to 3.7 μm (linewidth $\approx$6 cm^{-1}), both having a 15 ps pulse width and a 20 Hz repetition rate, are overlapped at the sample surface with incidence angles $\beta_{VIS}=45°$ and $\beta_{IR}=57°$, respectively, and the SFG output is detected in the reflected direction. The acetone liquid (99.9+% HPLC grade) is purchased from Aldrich Chemical Co., Inc.

The surface SFVS spectra in SSP, SPS, and PPP polarization combinations are shown in Fig. 6. All the measured SFVS signals have been calibrated with a reference *z*-cut quartz crystal, yielding for each polarization combination a spectrum of $|\chi_{eff}|^2$ in MKS units. In the CH stretch region, only one resonance peak at 2926 cm^{-1} is observed, and can be assigned to the CH symmetric stretch modes (Q_2 and Q_5). The peak strength is about five times stronger in SSP than in PPP. The signal in SPS is below the noise level, which is about 10 times smaller than the peak signal in SSP. The PSS spectrum is similar to SPS [Eq. (5)], and is not shown here.

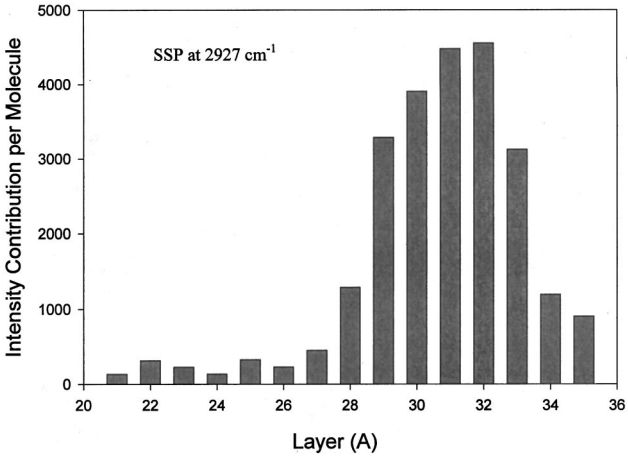

FIG. 5. The calculated SFG contribution from acetone molecules in various slabs at different depths parallel to the surface. The Gibb's dividing surface is at 32.2 Å.

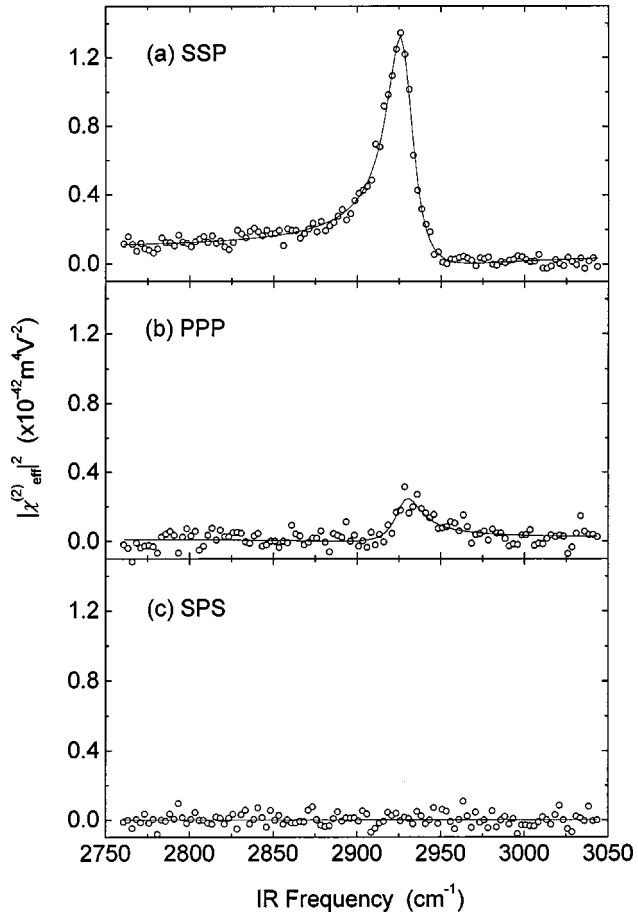

FIG. 6. The reflective SFG spectra of the liquid/vapor interface of acetone in the CH stretch region measured with three different polarization combinations; (a) SSP, (b) PPP, and (c) SPS. Solid lines in the figures are fits from Eqs. (3)–(5).

Within the electric–dipole approximation, SFG as a second-order nonlinear process is forbidden in the bulk of an isotropic medium. However, the magnetic–dipole and electric–quadrupole contributions from the bulk may not necessarily be negligible. It is important to check whether in our case, the observed SFVS spectra actually result from the acetone interface. We use the experimental scheme suggested by Xing *et al.*,[24] measuring SFG in both reflection and transmission directions. Because of the longer coherent length, the bulk contribution is much stronger in transmission than in reflection. Measurement of SFG in transmission allows an estimate of the bulk contribution. We find that the bulk contribution to SFG in reflection in the acetone case is negligible. This is expected from the general consideration for the CH stretch modes.[24]

We have also investigated the CO stretch mode. Within our detection limit, no resonance peak was observed in the IR region of 1600–1800 cm^{-1}. The result that the CH stretch is clearly observed but not the CO stretch indicates that the C═O vector either lies near the surface plane or points into

TABLE V. Surface tension of acetone and water at $T=20\,^{\circ}\mathrm{C}$ (Ref. 25).

	Acetone	Water
Surface free energy γ	$2.33\times10^{-2}\,\mathrm{J\,m^{-2}}$	$7.275\times10^{-2}\,\mathrm{J\,m^{-2}}$
Free energy per molecule γ/N_S	$5.7\times10^{-21}\,\mathrm{J}$	$7.0\times10^{-21}\,\mathrm{J}$

the liquid, and at least one methyl group is pointing away from the bulk. This is consistent with the simulation result.

IV. DISCUSSIONS

Except for some quantitative details, the calculated spectra agree well with the measured ones. (The discrepancy between theory and experiment in the PPP spectra is due to high sensitivity of the spectrum to the beam geometry.) We therefore believe that our MD simulation gives a reasonable picture of the liquid/vapor interfacial structure of acetone. The acetone surface appears to have a more ordered structure than that of the bulk. This is expected from the surface tension measurement of acetone.[25] The free energy per molecule at the free acetone surface is found to be comparable to that at the free water surface (see Table V). Since the surface tension of water is known to arise from the relatively strong OH···O hydrogen bond at the surface, the comparable surface free energy per molecule of acetone indicates a similarly strong molecular interaction at the acetone surface. Like water, the strong molecular interaction results in a more ordered structure at the surface than that in the bulk.

For crystalline acetone, the molecular interactions are dominated by the C═O···C═O and CH···O contacts. As revealed in the recent x-ray diffraction study,[26] crystalline acetone has an ordered layered structure. Within each layer, the C═O bond of each acetone molecule is nearly parallel to the layer plane ($\theta\sim90°$) and the CCC plane perpendicular to the layer plane ($\varphi\sim90°$). Each acetone molecule is surrounded by six other acetone molecules and the C═O bonds are aligned in the way either antiparallel or perpendicular to each other. The MD simulation discussed in the following paragraph suggests that in liquid the former is preferred. This arrangement results from the strong in-plane dipolar C═O···C═O interaction[27] as well as the CH···O contacts. The interaction between molecules from neighboring layers is relatively weak. At the liquid/vapor interface, we expect that the structure resembles that of an acetone crystalline layer although certainly not as highly ordered.

Another interesting result we find here is the predominant orientation of the nearest neighbors of surface molecules. From the previous simulations of Jedlovszky[28] and Rios[29] in bulk acetone, we know that the nearest neighbors prefer an antiparallel arrangement around the central molecule. When the coordination number increases, the distribution approaches a random behavior very rapidly. To obtain some information about the predominant orientation of the nearest neighbors of surface acetone molecules, we have calculated the cosine distribution of angle γ between the CO bonds of nearest neighbor molecules at the surface. Figure 7 shows the distribution of $\cos\gamma$ of surface molecules and compares it with those in the bulk. In the case of just the nearest neighbors, the distributions show clearly the preference for antiparallel orientation for both bulk and surface molecules. Also, they exhibit nearly identical results. It suggests that the interaction between nearest neighbors is nearly the same for surface and bulk acetone molecules. This is perhaps not surprising since Dang and Feller[30] also found the interactions between benzene–interfacial water and benzene–bulk water to be similar. When the coordination number increases in the bulk, the distribution tends to be more random, as shown by the squared curve in Fig. 7.

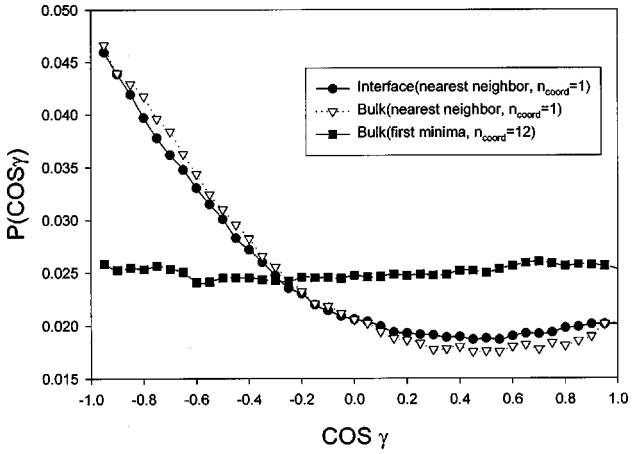

FIG. 7. The calculated distribution of $\cos\gamma$ with the angle γ being between the C═O bonds of nearest neighbor acetone molecules at 300 K. Circles are for the reflective orientation of nearest neighbor molecules (with coordination number $n_{\mathrm{coord}}=1$) at the surface. Triangles are for relative orientation of the nearest neighbor molecules ($n_{\mathrm{coord}}=1$) in the bulk. Squares are for the relative orientation of the first coordination shell ($n_{\mathrm{coord}}=12$) in the bulk.

V. CONCLUSIONS

In summary, molecular dynamics simulations have been used to calculate the molecular orientational distribution at the liquid/vapor interface of acetone. Then, in conjunction with the molecular theory of SFVS, the calculation allows us to compute the SF vibrational spectra of the acetone vapor/liquid interface. We obtain spectra dominated by the symmetric CH_3 stretch modes at 2926 $\mathrm{cm^{-1}}$, in good agreement with the experimental observation. The calculation then provides a picture for the structure of the acetone vapor/liquid interface: the surface acetone molecules prefer to have their molecular plane orient perpendicular to the surface, with the C═O vector pointing into the liquid bulk (nearly parallel to the surface) and one of the methyl groups protruding out of the bulk. This orientation is consistent with that of molecules in a layer plane of crystalline acetone. This observation together with the known strong surface tension of acetone, resulting from C═O···C═O interactions between neighboring molecules, indicates that the free acetone surface is highly ordered and crystal-like.

ACKNOWLEDGMENTS

We thank Professor C. Y. Mou (National Taiwan University) for stimulating discussions and Dr. Frederick J. Hollander (Chemistry Department, U.C. Berkeley) for access to

the CSD: Cambridge Structural Database, 1999. This work was supported by a grant from the National Science Council of ROC and the U.S. Department of Energy under Contract No. DE-AC03-76SF00098.

APPENDIX A: RELATION BETWEEN MOLECULAR COORDINATES AND LAB COORDINATES

The molecular coordinates are related to the lab coordinates by the linear transformation

$$\begin{pmatrix} \xi \\ \eta \\ \zeta \end{pmatrix} = \begin{pmatrix} \cos\varphi & \sin\varphi & 0 \\ -\sin\varphi & \cos\varphi & 0 \\ 0 & 0 & 1 \end{pmatrix} \begin{pmatrix} \cos\theta & 0 & -\sin\theta \\ 0 & 1 & 0 \\ \sin\theta & 0 & \cos\theta \end{pmatrix} \times \begin{pmatrix} \cos\phi & \sin\phi & 0 \\ -\sin\phi & \cos\phi & 0 \\ 0 & 0 & 1 \end{pmatrix} \begin{pmatrix} x \\ y \\ z \end{pmatrix}, \tag{A1}$$

where (θ,φ,ϕ) are the three angles defined in Fig. 1(b).

We can evaluate the products $(\mathbf{i}\cdot\mathbf{l})(\mathbf{j}\cdot\mathbf{m})(\mathbf{k}\cdot\mathbf{n})$ and find $K_{q,ijk}$ explicitly following Eq. (2). Taking $K_{q,yyz}$ with $q=1$ and 2, for example,

$$K_{q,yyz} = \left\langle \left(\frac{\partial \mu_\zeta}{\partial Q_q}\right) \cos\theta \left[\left(\frac{\partial \alpha_{\xi\xi}}{\partial Q_q}\right) (\cos\theta \sin\phi \cos\varphi + \cos\phi \sin\varphi)^2 + \left(\frac{\partial \alpha_{\eta\eta}}{\partial Q_q}\right) (-\cos\theta \sin\phi \sin\varphi + \cos\phi \cos\varphi)^2 + \left(\frac{\partial \alpha_{\zeta\zeta}}{\partial Q_q}\right) \sin^2\theta \sin^2\phi \right] \right\rangle. \tag{A2}$$

Similarly, for $q=4$ and 5,

$$K_{q,yyz} = 2\left(\frac{\partial \mu_\eta}{\partial Q_q}\right)\left(\frac{\partial \alpha_{\eta\zeta}}{\partial Q_q}\right) \langle \sin^2\theta \sin\varphi \sin\phi \times (-\cos\theta \sin\phi \sin\varphi + \cos\phi \cos\varphi) \rangle, \tag{A3}$$

and for $q=6$, we find

$$K_{q,yyz} = -2\left(\frac{\partial \mu_\xi}{\partial Q_q}\right)\left(\frac{\partial \alpha_{\xi\zeta}}{\partial Q_q}\right) \langle \sin^2\theta \cos\varphi \sin\phi \times (\cos\theta \sin\phi \cos\varphi + \cos\phi \sin\varphi) \rangle. \tag{A4}$$

For $q=3$, $K_{q,yyz}=0$ because $\partial\mu_n/\partial Q_q = 0$ with $n=\xi,\ \eta,\ \zeta$ (Table III). Other components like $K_{q,zzz}$ and $K_{q,yzy}$ can be obtained in the same way.

APPENDIX B: OVERALL LOCAL-FIELD CORRECTION FACTORS

The overall local-field correction factors in Eq. (5) are given by $L_{ii}(\Omega) = L'_{ii}(\Omega) l_{ii}(\Omega)$, where $L'_{ii}(\Omega)$ is the Fresnel coefficient and $l_{ii}(\Omega)$ is the microscopic local-field correction factor at the liquid/vapor interface. They are calculated following Ref. 20 and listed in the following table with other relevant parameters. The values of refractive indices at $T = 20\,^\circ\mathrm{C}$ are taken from Ref. 31.

	SF	VIS	IR
λ (wavelength)	0.460 μm	0.532 μm	3.418 μm
n (refractive index)	1.359	1.359	1.349
β (beam angle)	46.5°	45.0°	57.0°
L'_{xx}	0.949	0.941	1.032
L'_{yy}	0.749	0.757	0.680
L'_{zz}	1.051	1.059	0.968
$l_{xx}=l_{yy}$	1.141	1.141	1.137
l_{zz}	0.847	0.847	0.850

[1] I. Benjamin, Chem. Rev. **96**, 1449 (1996), and references therein.
[2] Q. Du, R. Superfine, E. Freysz, and Y. R. Shen, Phys. Rev. Lett. **70**, 2313 (1993).
[3] Y. R. Shen, Science **276**, 1520 (1997).
[4] X. Su, L. Lianos, Y. R. Shen, and G. A. Somorjai, Phys. Rev. Lett. **80**, 1533 (1998).
[5] I. Benjamin, Phys. Rev. Lett. **73**, 2083 (1994).
[6] I. Benjamin, J. Chem. Phys. **110**, 8070 (1999).
[7] S. H. Lin and A. A. Villaeys, Phys. Rev. A **50**, 5134 (1994); A. Morita and J. T. Hynes, preprint submitted to Elsevier Preprint (March 2000).
[8] P. Jedlovszky and G. Palinkas, Mol. Phys. **84**, 217 (1995).
[9] W. L. Jorgensen, J. M. Briggs, and M. L. Contreras, J. Phys. Chem. **94**, 1683 (1990).
[10] M. Ferrario, M. Hayghney, I. R. McDonald, and M. L. Klein, J. Chem. Phys. **93**, 5156 (1990).
[11] Y. L. Yeh and C. Y. Mou, J. Phys. Chem. B **103**, 3699 (1999).
[12] J.-P. Ryckaert, G. Ciccotti, and H. J. C. Berendsen, J. Comput. Phys. **23**, 327 (1977).
[13] M. P. Allen and D. J. Tildesley, *Computer Simulations of Liquids* (Oxford University Press, New York, 1987).
[14] H. J. C. Berendsen, J. P. M. Postama, W. F. van Gunsteren, A. DiNola, and J. R. Haak, J. Chem. Phys. **81**, 3684 (1984).
[15] J. Alejandre, D. J. Tildesley, and G. A. Chapela, J. Chem. Phys. **102**, 4574 (1995).
[16] G. A. Chapela, G. Saville, S. M. Thompson, and J. S. Rowlinson, J. Chem. Soc., Faraday Trans. 2 **8**, 133 (1977).
[17] C. A. Croxton, *Statistical Mechanics of The Liquid Surface* (Wiley, New York, 1980).
[18] G. J. Simpson and K. L. Rowlen, J. Phys. Chem. B **103**, 3800 (1999).
[19] P. B. Miranda and Y. R. Shen, J. Phys. Chem. B **103**, 3292 (1999).
[20] X. Zhuang, P. B. Miranda, D. Kim, and Y. R. Shen, Phys. Rev. B **59**, 12 632 (1999).
[21] P. Cossee and J. H. Schachschneider, J. Chem. Phys. **44**, 97 (1966).
[22] D. W. Liao, A. M. Mebel, M. Hayashi, Y. J. Shiu, Y. T. Chen, and S. H. Lin, J. Chem. Phys. **111**, 205 (1999).
[23] Y. R. Shen, in *Proceedings of the International School of Physics ''Enrico Fermt,'' Course CXX, Frontier in Laser Spectroscopy*, edited by T. W. Hänsch and M. Inguscio (North-Holland, Amsterdam, 1994), p. 139.
[24] X. Wei, S. C. Hong, A. I. Lvovsky, H. Held, and Y. R. Shen, J. Phys. Chem. B **104**, 3349 (2000).
[25] *Landolt–Börnstein II-3* (Springer-Verlag, Berlin, 1956), pp. 421, 426.
[26] D. R. Allan, S. J. Clark, R. M. Ibberson, S. Parsons, C. R. Pulham, and L. Sawyer, Chem. Commun. (Cambridge) **X**, 751 (1999).
[27] F. H. Allen, C. A. Baalham, J. P. M. Lommerse, and P. R. Raithby, Acta Crystallogr., Sect. B: Struct. Sci. **54**, 320 (1998).
[28] P. Jedlovszky and G. Palinkas, Mol. Phys. **84**, 217 (1995).
[29] J. M. Hermida-Ramon and M. A. Rios, J. Phys. Chem. A **102**, 2594 (1998).
[30] L. X. Dang and D. Feller, J. Phys. Chem. B **104**, 4403 (2000).
[31] J. E. Bertie and Z. Lan, J. Chem. Phys. **103**, 10 152 (1995).